Dynamical study of the spin Hall effect from interchain polaron hopping in organics

Yuanyuan Miao,[1,2] Huiqing Zhang,[1] Han Ma,[1] Huixin Li,[1] Junfeng Ren,[1] and Guichao Hu[1,*]
[1]*School of Physics and Electronics, Shandong Normal University, Jinan 250100, China*
[2]*School of Information Science and Engineering, Shandong Agricultural University, Taian 271018, China*

(Received 21 July 2023; revised 8 November 2023; accepted 8 January 2024; published 23 January 2024)

Using an extended Su-Schrieffer-Heeger model including spin-orbit coupling and a nonadiabatic dynamics method, the dynamic picture of spin Hall effect (SHE) from interchain hopping of polarons is revealed in a finite organic polymer ladder. The results demonstrate that the transverse hopping of the polaron between chains under an electric field causes a spin-resolved longitudinal motion of the polaron along the chain. The direction of longitudinal transport remains opposite for the initial spin-up and spin-down polarons, which induces a pure spin current carried by polarons. By means of the statistical average over two kinds of polarons with different initial spins, an obvious oscillating SHE is achieved. Spectrum analysis from Fourier transform of spin signal shows a low-frequency part and a high-frequency part in the spectrum. The low-frequency part is attributed to the intrinsic electron dynamic oscillation in the finite-size system in the presence of polarons and the adopted periodic boundary, and the high-frequency part is due to the spin-flip spin dynamics. In addition, we found that the charge-spin conversion efficiency from the interchain polaron hopping may be larger than that from the intrachain polaron transport by one order, which confirms the enhancement of charge-spin conversion efficiency by organic anisotropy. This work deepens our understanding on the mechanism of organic SHE from polarons hopping, as well as the merit of organic anisotropy in the realization of a large SHE.

DOI: 10.1103/PhysRevB.109.014314

I. INTRODUCTION

The spin Hall effect (SHE) [1–5] is an effective way to generate a spin current via an electric current in spin-orbit coupling (SOC) systems. Its reciprocal inverse, the inverse spin Hall effect (ISHE) [6–9], also realizes the generation of an electric current by a spin current. The spin-charge conversion originating from these effects has attracted extensive attention in past decades, where the materials involved are usually limited to inorganic metals and semiconductors because of the inherent large atomic SOC strength [4,6,10–21]. In recent years, spin-charge conversion in π-conjugated organic materials is rising as an intriguing topic. Organic materials are known in spintronics for their merits of low-processing cost, flexible structure, and long spin-relaxation time. Despite that, the realization of distinct SHE in organic materials remains challenging due to the weak atomic SOC from light atomic components. Although a few works have indicated that the effective SOC in organics can be greatly enhanced by doping heavier atoms or conformation distortion [22–30], exploring the microscopic picture of organic SHE based on its unique characteristics is necessary and urgently required, but is less involved to date.

Unlike inorganics, the electron-lattice (e-l) coupling in organic materials is strong, which makes the carriers in organics as a series of localized excitations, such as solitons, polarons, and bipolarons [31,32]. Polarons are common spin/charge carriers formed by an extra electron (hole) bound by lattice distortions, which are believed to play a crucial role in organic spin-charge conversion. For example, Watanabe *et al.* [33] found that a pure spin current can be conducted through polarons in conjugated organic poly(2,5-bis(3-alkylthiophen-2-yl)thieno[3,2-b]thiophene), which contributes to the subsequent ISHE. Ando *et al.* [34] reported the ISHE in poly(3,4-ethylenedioxyethiophene) molecules doped by poly(4-styrenesulphonate). Other related experimental works about the ISHE in organics were also performed in the predoped condition [35–37], where the formation of polarons is expected. On the theoretical side, the SHE from polaron transport is rarely involved. The pioneering work of organic SHE is limited to the electron transport in disordered organic solids with a master-equation method [38]. The study of a pure spin current assisted by spin exchange of polarons [39] or hopping of polarons [40] has been carried out by using spin diffusion theory, but the SHE is not considered. Recently, by employing an extended Su-Schrieffer-Heeger (SSH) model [41] and a nonadiabatic dynamics method, the microscopic dynamic process of the SHE from polaron and bipolaron intrachain transport has been revealed [42,43], where a prominent oscillating SHE is found and a new mechanism of skew scattering caused by lattice distortion was proposed.

Besides the strong e-l interaction, another characteristic of organic polymers is the anisotropy conductance, which is caused by the much stronger intrachain coupling ($\sim$2.5 eV) than the interchain coupling ($\sim$0.1 eV). Interchain hopping of polarons is inevitable in experiments because of the finite length of organic chains, the alignment of polymers, or the nonzero angle to the organic chain of the applied electric field. In past decades, the dynamics of interchain polaron hopping between polymer chains has been investigated

*Corresponding author: hgc@sdnu.edu.cn

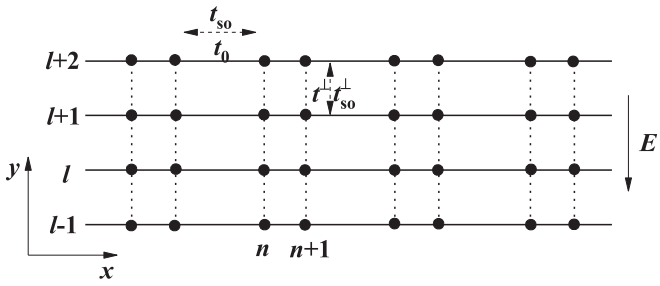

FIG. 1. Schematic of the coupled organic chains.

[44,45], where a different picture from the bandlike intrachain polaron transport was revealed. For example, in the case of intrachain transport the polaron is accelerated by the field and then moves with a saturation velocity, whereas the interchain transport of polarons takes the form of hopping, which depends on the strength of field and interchain coupling. When the SOC is included and the issue of SHE is concerned, such different transport scheme is expected to give a distinct spin-charge conversion picture, which has not been explored. Ando *et al.* have mentioned that in their ISHE experiment the anisotropy of organics is helpful to enhance the spin-charge conversion efficiency [34], while the details still remain obscure. In this work, with the aim of clarifying the dynamic details of SHE from interchain polaron hopping, we performed numerical simulations of interchain polaron hopping through several coupled organic chains in the presence of SOC. With the widely used nonadiabatic dynamic method [46,47], the microscopic picture of the SHE is explored, and the spin-charge conversion efficiency is discussed, which is further compared with the SHE from intrachain polaron transport. The remainder of this paper is organized as follows: In Sec. II, the model and the details of the theoretical method are introduced. In Sec. III, the results of the numerical calculations are presented and analyzed. A brief summary is given in Sec. IV.

II. MODEL AND METHOD

As shown in Fig. 1, we consider a system consisting of several coupled polymer chains aligned along the x direction. A transverse electric field of strength E along the negative y direction is applied to drive the polaron hopping between chains. The system is described by extending the well-known SSH model including the SOC and the electric field term. The Hamiltonian is given by

$$H(t) = H_0 + H_{\rm so} + H_{\rm latt} + H_E(t). \tag{1}$$

Here, H_0 is the electron hopping in the framework of the tight-binding model, which is written as

$$H_0 = -\sum_{l,n,\sigma} t^l_{n,n+1}(c^\dagger_{l,n+1,\sigma}c_{l,n,\sigma} + \text{H.c.}) - t^\perp \sum_{l,n,\sigma}(c^\dagger_{l+1,n,\sigma}c_{l,n,\sigma} + \text{H.c.}), \tag{2}$$

where $t^l_{n,n+1} = t_0 - \alpha(u_{l,n+1} - u_{l,n})$ is the intrachain hopping integral of π electrons between site n and $n+1$ of the lth chain. t_0 is the transfer integral for a uniform chain. α is the e-l coupling constant, and $u_{l,n}$ is the lattice displacement along the chain at the nth site of the lth chain. $c^\dagger_{l,n,\sigma}(c_{l,n,\sigma})$ denotes the electron creation (annihilation) operator at site n of the lth chain with spin σ. $t^\perp$ is the transverse interchain hopping integral between the chain l and $l+1$ at the nth site, where the lattice displacement along the transverse direction is not considered in the present model.

$H_{\rm so}$ describes the Hamiltonian for the Rashba SOC effect. Using a tight-binding model, it can be written as

$$H_{\rm so} = -t_{\rm so}\sum_{l,n,\sigma,\sigma'}[c^\dagger_{l,n+1,\sigma'}(i\sigma_y)c_{l,n,\sigma} + \text{H.c.}] + t^\perp_{\rm so}\sum_{l,n,\sigma,\sigma'}[c^\dagger_{l+1,n,\sigma'}(i\sigma_x)c_{l,n,\sigma} + \text{H.c.}]. \tag{3}$$

Here, $t_{\rm so}$ and $t^\perp_{\rm so}$ represent the strengths of intrachain and interchain SOC, respectively. σ_x and σ_y are the Pauli matrices.

The third term, $H_{\rm latt}$, is the lattice elastic energy and kinetic energy described as

$$H_{\rm latt} = \frac{K}{2}\sum_{l,n}(u_{l,n+1} - u_{l,n})^2 + \frac{M}{2}\sum_{l,n}\dot{u}^2_{l,n}, \tag{4}$$

where K is the elastic constant and M is the mass of a CH monomer.

The last term gives the contribution of the transverse electric field to the Hamiltonian, which reads

$$H_E(t) = -|e|E(t)b\sum_{l,n,\sigma}\left(l - \frac{J+1}{2}\right)c^\dagger_{l,n,\sigma}c_{l,n,\sigma} + |e|E(t)b\sum_{l,n}\left(l - \frac{J+1}{2}\right). \tag{5}$$

Here, e is the elementary charge; b is the lattice constant along the transverse direction, which is chosen as 4.24 Å [45]; and J is the total number of chains. The electric field $E(t)$ is set as a constant after a turn-on time, which is applied in the following way:

$$E(t) = \begin{cases} E_0 \exp\left[-(t-t_c)^2/t_w^2\right] & \text{for } t < t_c \\ E_0 & \text{for } t \geqslant t_c, \end{cases} \tag{6}$$

where $t_c = 75$ fs is the center, $t_w = 25$ fs is the width, and E_0 is the strength of the Gaussian.

Before the dynamical simulation, the initial state of the system is first determined without the electric field. The electron eigenstate $|\psi_\mu\rangle$ is expanded in Wannier space as $|\psi_\mu\rangle = \sum_{l,n,\sigma}\psi^\mu_{l,n,\sigma}|l,n,\sigma\rangle$. μ is the index of energy level and $\psi^\mu_{l,n,\sigma}$ is the wave function at the site (l,n) with spin σ. The wave function and stable lattice configuration can be obtained by solving the electronic eigenequation and lattice equilibrium equation [42]. A periodic boundary condition along the x direction is used for each chain to trace the long-time transport of polarons. The time evolution of the electronic state can be simulated by solving the time-dependent

Schrödinger equation

$$i\hbar\frac{\partial}{\partial t}\psi^{\mu}_{l,n,\sigma} = -t^{l}_{n-1,n}\psi^{\mu}_{l,n-1,\sigma} - t^{l}_{n,n+1}\psi^{\mu}_{l,n+1,\sigma} - t^{\perp}\psi^{\mu}_{l-1,n,\sigma} - t^{\perp}\psi^{\mu}_{l+1,n,\sigma} - t_{\mathrm{so}}\big(\psi^{\mu}_{l,n-1,\uparrow}\delta_{\sigma,\downarrow} - \psi^{\mu}_{l,n-1,\downarrow}\delta_{\sigma,\uparrow} + \psi^{\mu}_{l,n+1,\downarrow}\delta_{\sigma,\uparrow} - \psi^{\mu}_{l,n+1,\uparrow}\delta_{\sigma,\downarrow}\big) + it^{\perp}_{\mathrm{so}}\big(\psi^{\mu}_{l-1,n,\uparrow}\delta_{\sigma,\downarrow} + \psi^{\mu}_{l-1,n,\downarrow}\delta_{\sigma,\uparrow} - \psi^{\mu}_{l+1,n,\downarrow}\delta_{\sigma,\uparrow} - \psi^{\mu}_{l+1,n,\uparrow}\delta_{\sigma,\downarrow}\big) + |e|E(t)\left(l - \frac{J+1}{2}\right)b\psi^{\mu}_{l,n,\sigma}. \tag{7}$$

Here $\delta_{\sigma,\uparrow(\downarrow)} = 1$ for $\sigma = \uparrow$ $(\downarrow)$ and otherwise equals zero.

The classical Newton's equation of motion is used for the evolution of lattice displacements

$$M\ddot{u}_{l,n}(t) = 2\alpha\mathrm{Re}\big[\big(\rho^{l}_{n,n+1} - \rho^{l}_{n-1,n}\big)\big] - K(2u_{l,n} - u_{l,n+1} - u_{l,n-1}). \tag{8}$$

Here $\rho^{l}_{n,n'} = \rho^{l}_{n,n',\uparrow} + \rho^{l}_{n,n',\downarrow}$ is the density matrix. In the mean-field approximation the elements of the density matrix are described by $\rho^{l}_{n,n',\sigma} = \sum_{\mu}\psi^{\mu*}_{l,n,\sigma}f_{\mu,\sigma}\psi^{\mu}_{l,n',\sigma}$. $f_{\mu,\sigma}$ is the time-independent distribution function determined by initial occupation (being 0,1). Equations (7) and (8) can be solved numerically with a Runge-Kutta method of order eight with step-size control [48], which is an effective approach to study the polaron dynamics in organic polymers [49,50]. The time step is taken as 1 fs. The time-dependent charge density $Q_{l,n}(t)$ and spin density $S^{z}_{l,n}(t)$ along the z axis at each site can be further defined as

$$Q_{l,n}(t) = 1 - \rho^{l}_{n,n}(t), \tag{9}$$

$$S^{z}_{l,n}(t) = \frac{\hbar}{2}[\rho^{l}_{n,n,\uparrow}(t) - \rho^{l}_{n,n,\downarrow}(t)]. \tag{10}$$

The parameters of the model are chosen for *trans*-polyacetylene [42,51], $t_0 = 2.5$ eV, $\alpha = 4.1$ eV/Å, $K = 21.0$ eV/Å^2, and $M = 1349.14$ eV fs^2/Å^2. The obtained results are expected to be valid qualitatively for other conjugated polymers. Limited by the cost of numerical calculation, the system is set as five coupled chains with $N = 160$ sites for each chain. The interchain hopping integral is taken as $t^{\perp} = 0.08$ eV, which is a reasonable value adopted for organic polymers [44,45]. The strength of the SOC is used as $t_{\mathrm{so}} = 2t^{\perp}_{\mathrm{so}} = 0.02$ eV. Although the SOC in organics is usually weak due to the light-element component, e.g., 11 cm^{-1} for carbon atoms [30], an effective SOC can still be achieved due to the presence of heavy atoms, such as S (382 cm^{-1}) in sexithiophene and Al (112 cm^{-1}) in Alq_3 [30]. Additionally, even in metal-free molecules it has been reported that the SOC may be enhanced by several orders of magnitude via the structural conformation [28,29]. The slightly larger SOC adopted here is useful to make the picture clearly visible, while the obtained results hold qualitatively even a smaller SOC is used. The strength of the electric field is $E_0 = 6.0$ mV/Å.

III. RESULTS AND DISCUSSION

In the initial state, we assume that a full spin-polarized polaron along the z axis is localized in the center of the lowest chain (chain 1). Here two kinds of energetically degenerate polarons, spin-up and spin-down polarons, are considered, respectively, since their dynamics will be not degenerate due to the presence of SOC. The polaron is realized by introducing an extra electron occupying the degenerate lowest unoccupied molecular orbital of chain 1 with up spin or down spin. After the dynamic simulation of each kind of polaron, a statistic average of the dynamic results for the two kinds of polarons will be performed. The aim is to meet the typical judging criteria in SHE experiments [16], where a pure spin current is generated by an unpolarized current. It is also reasonable since in nonmagnetic organic polymers the spin-up and spin-down polarons should be energetically degenerate and thus contribute equally to current. Such strategy has been proved valid in the study of the SHE from intrachain polaron transport [42].

Now we apply an electric field perpendicular to the chains with a strength of $E_0 = 6.0$ mV/Å. As shown in Fig. 2, the time evolution of the charge and spin densities for both kinds of polarons are given. In Figs. 2(a) and 2(b), one can find that the polaron initially localized on chain 1 quickly jumps to the center of chain 2 under the driving electric field, and after a few femtoseconds jumps to the next chain. At about 98 fs, the polaron reaches the last chain. Due to the boundary the polaron oscillates around the last chain. Eventually, an interchain polaron is obtained and distributed mainly on chains 3, 4 and 5, where a larger proportion remains on chain 4. Besides the interchain hopping, an interesting directional intrachain transport is observed for the polaron. The trajectory of the charges on each chain is opposite for the spin-up and spin-down polarons. The time evolution of the spin densities of the spin-up and spin-down polarons are shown in Figs. 2(c) and 2(d). The trajectory is similar to the polaron charge. In addition, an obvious spin flipping for the polaron is observed at around 1000 fs, which is caused by the SOC. Spin precession of polarons in the presence of SOC has been widely reported in the polaron dynamics along a polymer chain [52,53].

In order to get a more intuitive vision for the polaron hopping between the chains, we give the charge density distribution on each chain for the two kinds of polarons at different times. The results are shown in Fig. 3. In Fig. 3(a), at the initial time the charge densities of the spin-up and spin-down polarons overlap, which locate in the center of chain 1. At $t = 26$ fs in Fig. 3(b), the main body of the polaron arrives at chain 2 under the electric field, while fractional charges remain on chain 1 and some foregoing parts appear on the front chains. This means that the localized polaron changes into an interchain one during the hopping between chains. Slight nondegeneracy between the two kinds of polarons emerges for the charges on chain 5 due to the presence of SOC. With the increase of time the polaron continues to hop forward under the electric field, where the main body appears on chains 3, 4, and 5 in turn at $t = 36$, 55, and 98 fs. At $t = 105$ fs, the main

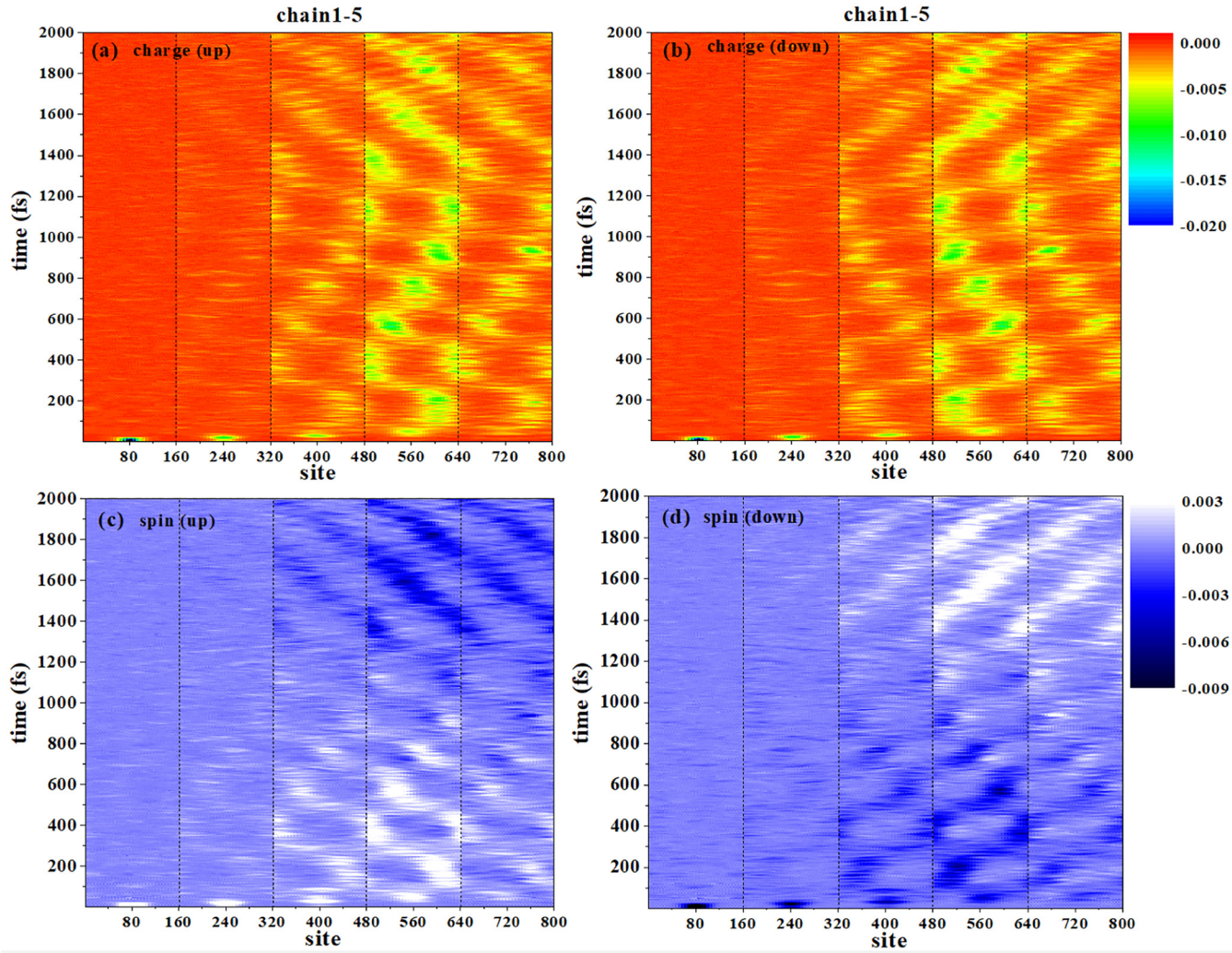

FIG. 2. Time evolution of the charge and spin densities of a polaron initially localized on chain 1. (a) and (b) show the charge densities for the spin-up and the spin-down polarons. (c) and (d) show the spin densities for the spin-up and the spin-down polarons.

body of the polaron is reflected to chain 4 due to the boundary. During the process of polaron hopping, we found that the nondegeneracy for the two kinds of polarons turns more pronounced, as shown in Figs. 3(c)–3(f). Moreover, the relative position of the spin-up and spin-down peaks exchanges after $t = 55$ fs. The above results indicate that under the transverse electric field, an opposite longitudinal motion occurs for the polarons with different initial spins in the presence of the SOC.

Due to the periodic boundary condition along the x direction, a long-time evolution of polarons along the chain is permitted. In the following, the intrachain motion of polarons is investigated in detail. Here we take chain 4 as an example. The case on other chains is similar in nature except for the quantity of charges. The time evolution of the charge density along the chain is plotted in Fig. 4 for the two kinds of polarons. After the initial time, the charges on chain 4 arise from zero and the polaron starts to emerge. An apparent polaron is obtained at 55 fs, where the polaron centers are shifted oppositely for the two kinds of polarons. At 65 fs, an obvious drift is observed for the polaron, which is to the right (left) for the spin-up (-down) polaron. This indicates the generation of a pure spin current along the chain. Such directional movement is still observed at $t = 100$ and 550 fs. However, as shown from Fig. 4(g) to Fig. 4(i), the movement direction of the polarons is reversed at long times from 1575 to 1810 fs. So, the interchain polaron hopping induces an oscillating spin current along the chain.

The continuous trajectory of the polaron on chain 4 can be traced through the time evolution of the polaron center. Here we define the polaron center P_c from the charge density as [50]

$$P_c = \begin{cases} N\theta/2\pi & \text{if } \langle\cos\theta \geqslant 0\rangle \text{ and } \langle\sin\theta \geqslant 0\rangle \\ N(\pi+\theta)/2\pi & \text{if } \langle\cos\theta\rangle < 0 \\ N(2\pi+\theta)/2\pi & \text{otherwise,} \end{cases} \tag{11}$$

with $\theta = \arctan[(\sum_n \rho_{n,n}^{l=4} \sin 2\pi n/N)/(\sum_n \rho_{n,n}^{l=4} \cos 2\pi n/N)]$. The definition of the polaron center is helpful to overcome the difficulty in determining the specific position of the polaron during dynamics caused by the width of the polaron

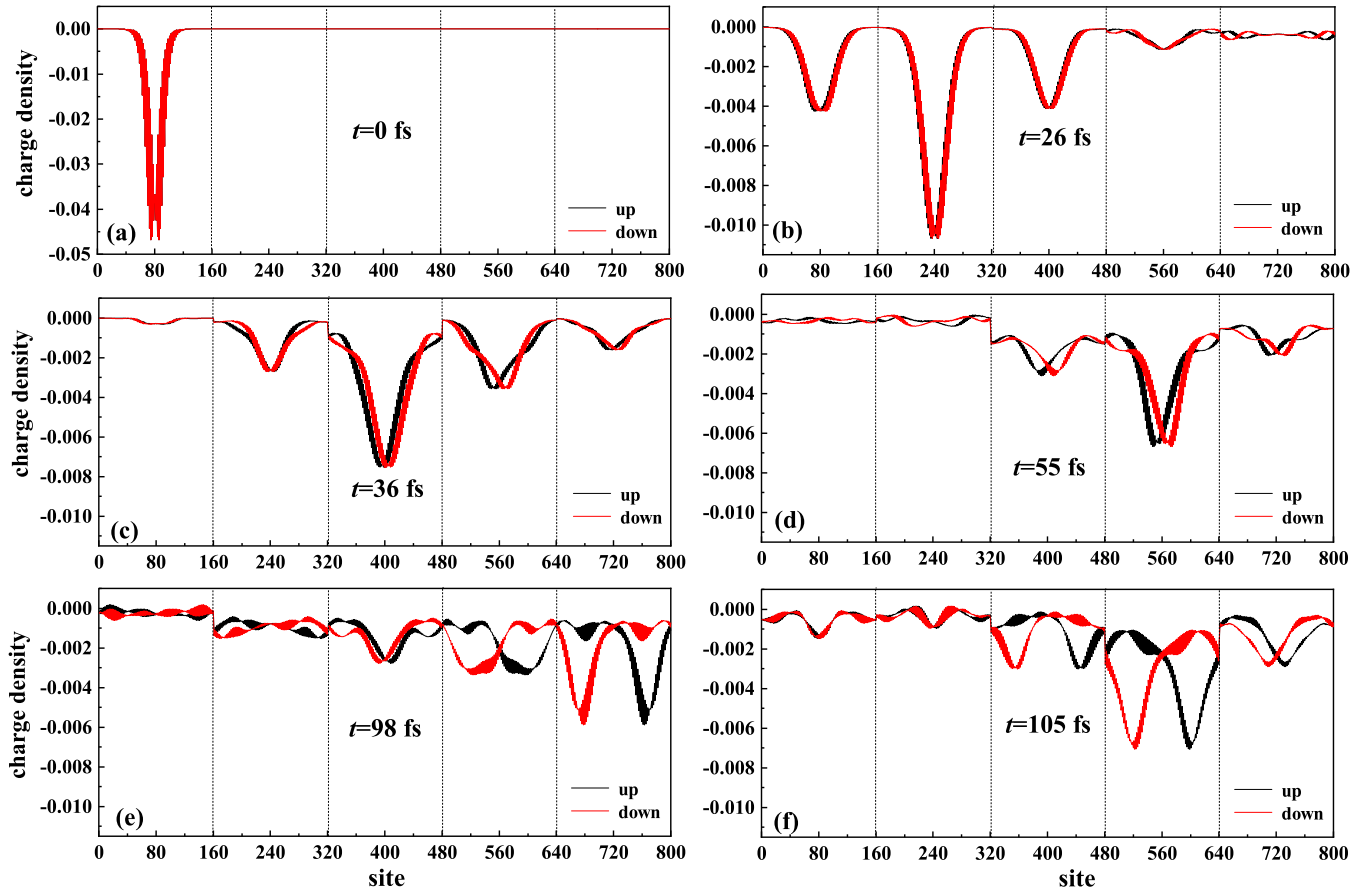

FIG. 3. Charge density on each chain at different times for the spin-up and spin-down polarons. The chains from 1 to 5 are aligned from the left to the right.

(∼40 sites). Thus, the trajectory of the polaron can be traced. For example, at the static state without field, the center of the polaron lies at the center of the lattice distortion. Figure 5(a) shows the trajectory of the spin-up polaron on chain 4. The motion of the spin-down polaron is opposite to the spin-up one, which is not shown anymore. In the initial 100 fs, the polaron drifts right from the 80th site to the 120th site, and then an irregular oscillation is followed up to 500 fs. From Fig. 2(a) we find that the oscillation of the longitudinal motion of the polaron occurs during the period of scattering by the boundary along the y direction. After that, the polaron wiggles to the right end of the chain at around 1000 fs. With a subsequent short oscillation, the transport direction of the polaron is reversed at around 1300 fs. From that time, the polaron moves periodically along the chain with a velocity of about 0.69 Å/fs. A second reversion of the transport direction happens at around 3300 fs. Figure 5(b) demonstrates the net spin on the chain with time. An obvious spin precession of the polaron between ± 0.3 is observed with a period of about 1500 fs, which is mainly caused by the intrachain SOC as reported in previous studies [42,52,53].

The above results reveal the details of polaron motion on one chain. To quantify the SHE of the whole system from the interchain hopping of polarons, one needs to clarify the evolution of the total charge and spin of the whole system. In the following, we investigate the evolution of total charge and spin in the left and right moieties. Specifically, the left moiety means the sum of 1–80 sites for every chain, and the right one is the sum of 81–160 sites. The results for both the spin-up and the spin-down polarons are shown in Fig. 6. In the initial state, the polaron locates at the center of chain 1, that is, the center of the 80th bond. Thus, the initial total charge and spin in each moiety is $0.5e$ and $\pm 0.5\hbar$ for the spin-up and spin-down polarons. As the polaron hops between chains, the total charges of the left and right parts oscillate with time around $0.5e$ due to the longitudinal motion of the polaron. The cases of the spin-up and spin-down polarons are antisymmetric. Besides the oscillation, the evolution of the total spin demonstrates a trend of spin precession.

As mentioned above, to meet the criteria of the SHE, that is, a longitudinal spin current generated by a transverse unpolarized charge current, we performed a statistical average over the two kinds of polarons. The time-dependent averaged total charge and spin in the left and right moieties are given in Figs. 7(a) and 7(b). It can be seen that the averaged charges of the left and right parts always remain zero at all times, which means the charge current only flows along the y direction. However, the averaged net spins in the two parts are opposite and oscillate irregularly with time. This indicates that an oscillating pure spin current along the x direction is generated. In other words, an oscillating SHE is truly obtained from the transverse hopping of the polarons.

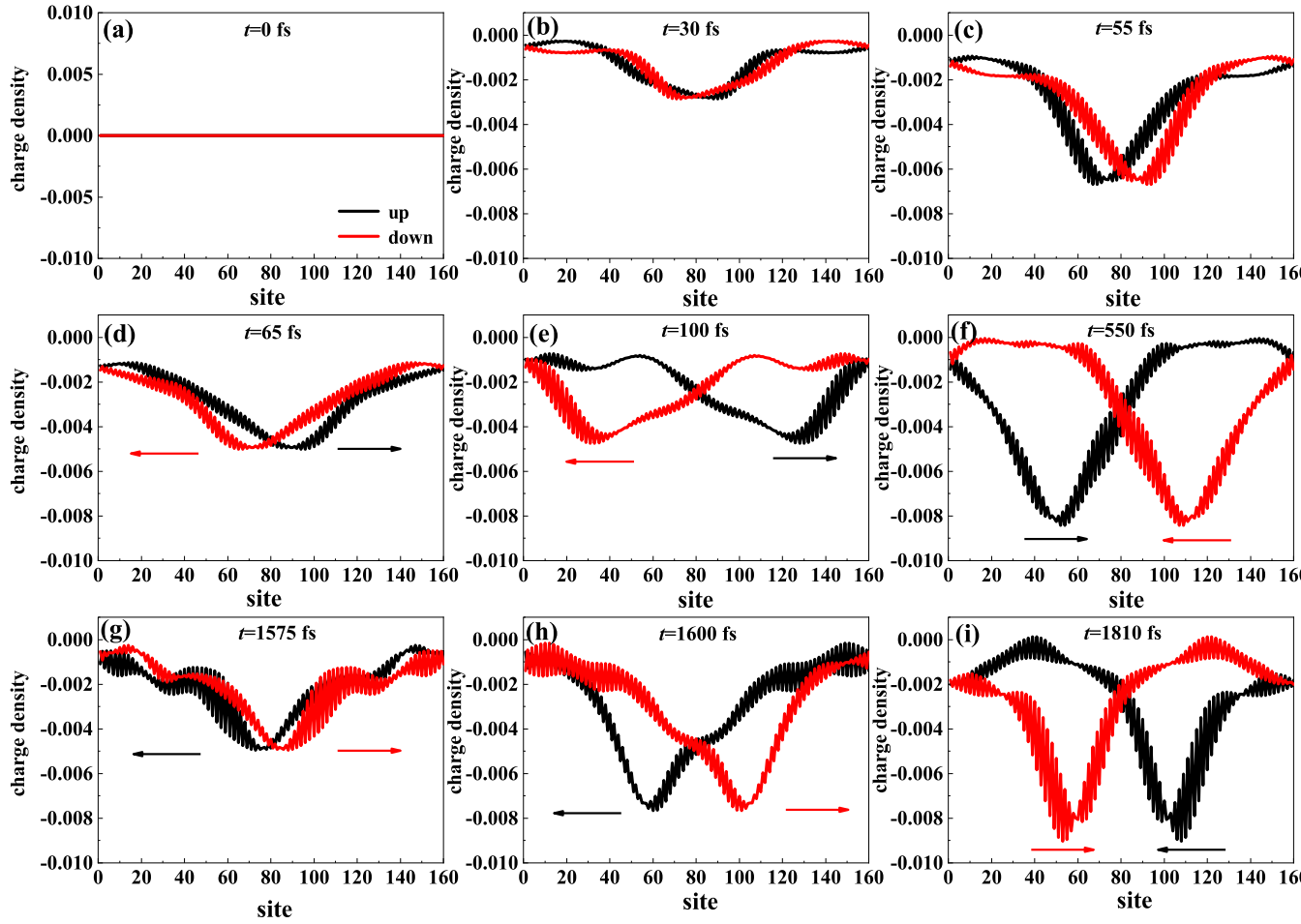

FIG. 4. Time evolution of charge density on chain 4 for polarons with different initial spins.

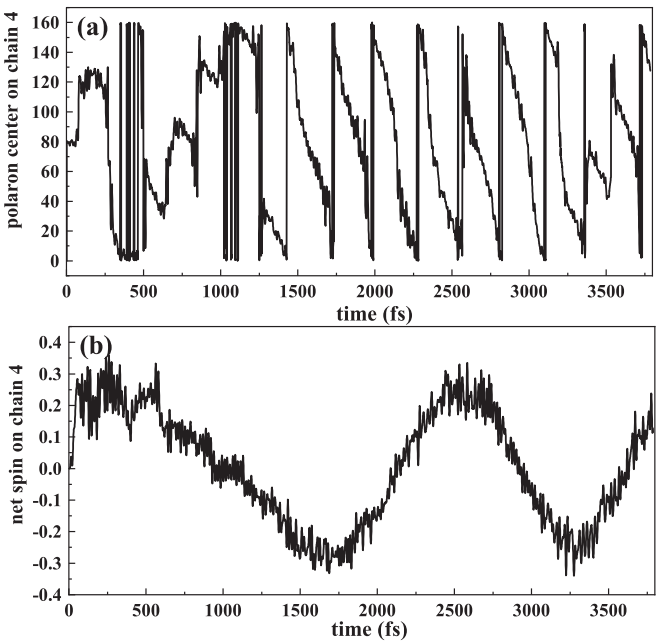

FIG. 5. (a) Center of the polaron on chain 4 as a function of time. (b) Spin procession of the polaron with time on chain 4.

The oscillation behaviors of the SHE can be further analyzed by the spectral analysis. In Fig. 8(a), we give the fast Fourier transform (FFT) of the time-dependent averaged spins in the left moiety of the system. We can see that the spectrum contains one low-frequency part below 0.1 fs^{-1} and one high-frequency part from 0.3 to 0.5 fs^{-1}. The oscillating property of the SHE in organic chains has been well analyzed in the previous study of intrachain polaron transport [42]. From that, the high-frequency part is induced by the spin-flip spin transfer caused by the SOC, and the low-frequency part is attributed to the intrinsic electron dynamic oscillation in the finite-size system in the presence of polarons, including the oscillation induced by boundary.

Here we would like to discuss the effect of boundary condition on the oscillation of the SHE in detail. In our model, the periodic boundary condition is used in the longitudinal direction, while in the transverse direction the boundary remains open. This is because polymers are quasi-one-dimensional materials, where the periodicity is apparent in the direction along the chain, but is inconspicuous in the direction perpendicular to the chain. The alignment and coupling between chains rely on the morphology of organics. Both the boundary conditions cause additional contribution to the oscillation of the SHE as analyzed below. In the transverse direction, the boundary bounce of polarons leads to a dynamic oscillation of charges around the edge, which naturally brings oscillation

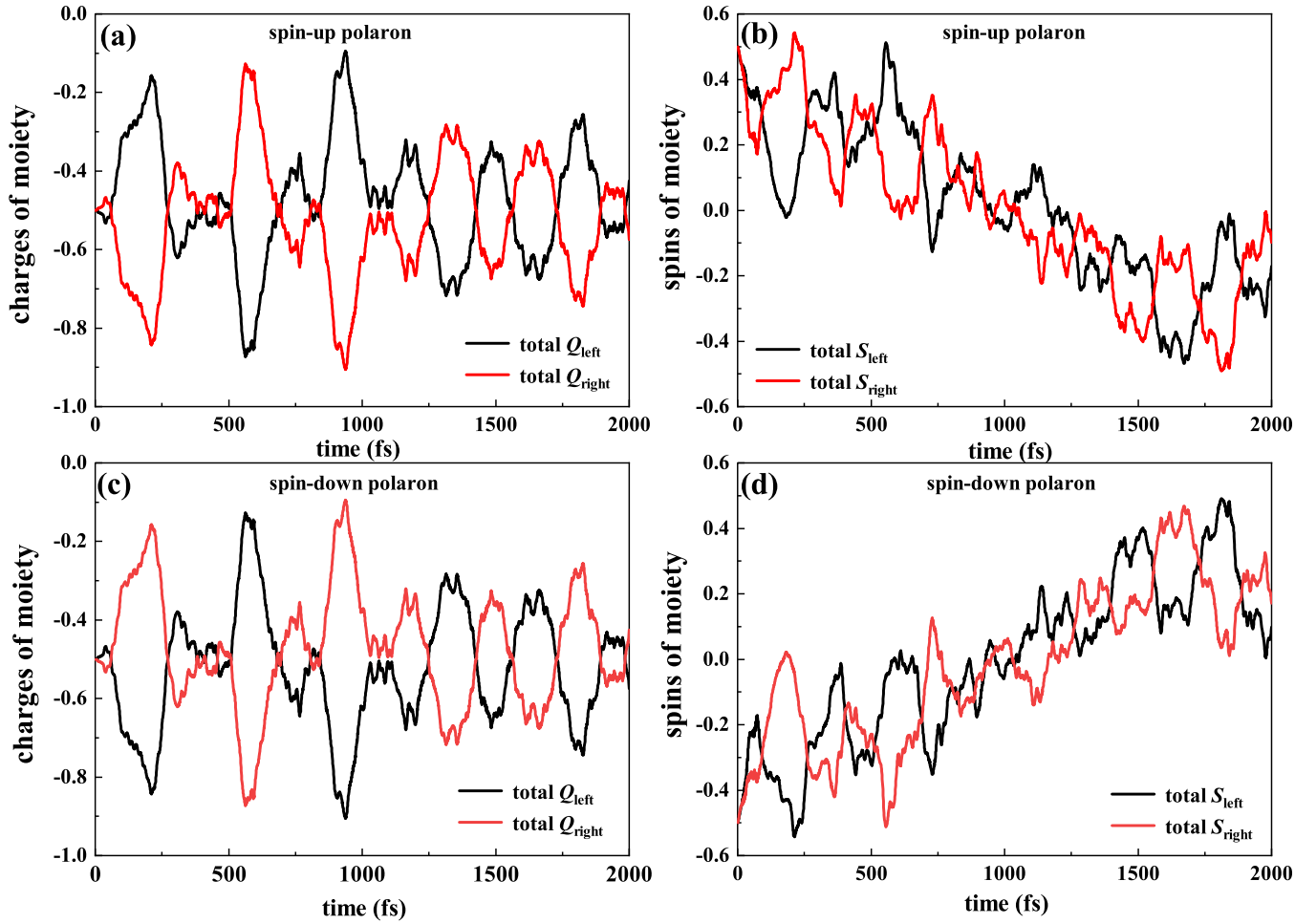

FIG. 6. Time evolution of the total charge and spin in the left and right moieties of the system. Here, the left moiety means the sum of 1–80 sites for every chain, and the right one is the sum of 81–160 sites. (a) and (b) show the charge and spin for the spin-up polaron. (c) and (d) show the charge and spin for the spin-down polaron.

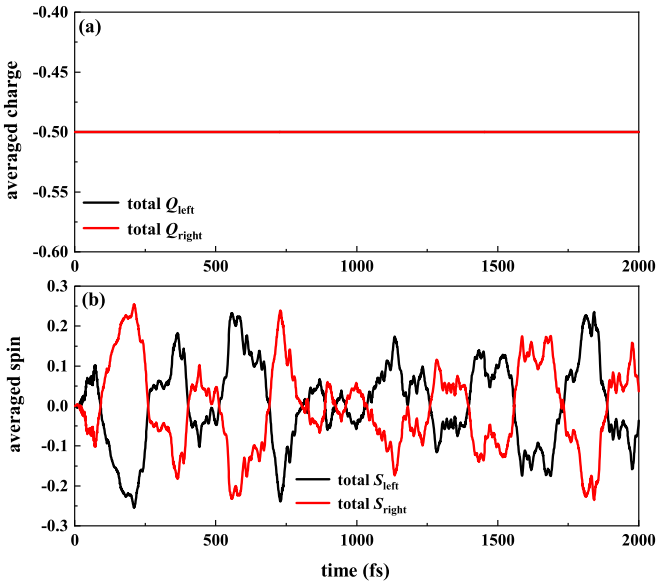

FIG. 7. (a) Total charges and (b) spins in the left and right moieties of the system after the statistic average over the spin-down and spin-up polarons.

to the converted spin current. To extract its contribution, we define the center of charges along the y direction as $y_c^Q(t) = [\sum_{j=1}^{5} q_j(t) y_j] / \sum_{j=1}^{5} q_j(t)$. $q_j(t)$ is the total charges on chain j at each time and $y_j = jb$ is the discrete coordinate of the chain. The time evolution of the charge center and its FFT are shown in Fig. 8(b). Obviously, a narrow low-frequency peak at about 0.01 fs^{-1} is obtained, which matches the extremely low-frequency peak in Fig. 8(a) with large amplitude quite well. The high-frequency branch above 0.3 in Fig. 8(a) is not observed in the charge oscillation, since it is actually contributed by spin-flip dynamics.

In the longitudinal direction, the use of periodic boundary condition will be helpful to trace long-time evolution of polarons, but the cyclic motion of spin-resolved polarons also leads to additional oscillation of the spin density in the left and right moieties of the system. The angular frequency can be roughly estimated from the periodic motion of the polaron center in chain 4 shown in Fig. 5(a). For example, the period of the cyclic motion in the interval between 1400 and 3400 fs is around 280 fs. According to our definition, such motion leads to an oscillation of the spin density in the left or right moiety with a period of about 140 fs, that is, an angular frequency of about 0.04 fs^{-1}. Such value falls in the low-frequency part.

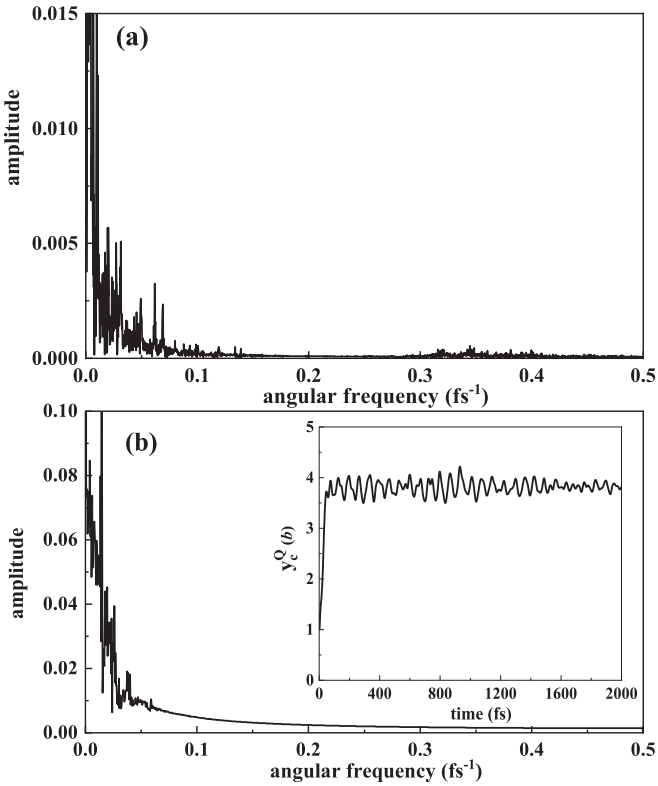

FIG. 8. (a) Fast Fourier transform (FFT) of the time evolution of the averaged spin in the left moiety. (b) FFT of the center of charge in the y direction. The inset is the time evolution of the center of charge in the y direction, where the vertical coordinate is the label of chains.

Considering the fluctuation of the longitudinal velocity of charges in different chains, it is believed that the extension of the low-frequency peak beyond 0.05 fs^{-1} should be relevant to the cyclic motion of the polaron. Despite that, here we would like to restate that the boundary is not the main reason for the oscillation behavior of the SHE in nature, but the presence of polarons and the related spin-flip dynamics. This is because the oscillation of spin density on chain 4 happens even before the arrival of a polaron to the boundary, as shown in Figs. 4(b)–4(d). Moreover, Ref. [42] has demonstrated that such fast oscillation will be absent in finite rigid chains without polarons.

Due to the presence of boundary the size effect is also investigated. Here the total chains in the y direction are increased to seven, and the site number in each chain is taken as $N = 160$ and 120, respectively. The time-dependent averaged spin and its FFT in each case are shown in Fig. 9. It is found that in the case of $N = 160$, the amplitude of the converted spin density is a little smaller than that in five chains, but the FFT curve is very similar. We even checked the case of nine chains (not shown here), where the situation is close to that of seven chains with a comparable magnitude of the averaged spin and similar FFT shape. When the chain length in the longitudinal direction is decreased to 120, the magnitude of the SHE does not change too much. However, a slight blueshift of the border of the low-frequency peak happens. This confirms that such frequency is truly relevant to the cyclic motion of polarons, since the period will be shortened and thus the frequency will be lifted in a shorter chain. The above results show that the boundary does not change the result too much.

Now let us compare the charge-spin conversion pictures caused by interchain hopping and intrachain transport of polarons. In the case of intrachain transport, which has been well studied in Ref. [42] with a three-chain system, the polarons are mainly confined in the central chain and move with a large saturation speed under the electric field. The converted pure spin current is contributed by fractional electrons extracted from the polarons by interchain coupling. Thus, therein the charge current is usually large but the spin current is small. However, in the case of interchain polarons hopping, a directional motion of the whole polaron occurs, which is opposite for the spin-up and spin-down ones. As a result, a much larger amplitude of the converted spin current is achievable, caused by a slow charge hopping. So, an enhanced SHE by organic anisotropy is achieved.

In the following, to quantify the effect of organic anisotropy on the SHE, we compared the charge-spin conversion efficiency of the SHE between longitudinal and transverse polaron transport. The system with five coupled chains is considered. For the longitudinal transport, the polaron initially locates at the center of chain 3, and the electric field is applied along the $-x$ direction. To make a comparison, the same parameters are necessary in the two cases. Since the electric field used above is too strong to dissociate the polaron in the case of intrachain transport, here a smaller strength of the electric field $E_0 = 0.1$ mV/Å is used. To make the results clearly visible, a relative larger SOC $t_{so} = 2t_{so}^{\perp} = 0.04$ eV is taken. Other parameters remain unchanged as above. In Fig. 10, we first give the spin density with time generated by the SHE in each case. It is found that the transverse polaron transport corresponds to larger amplitude, which is of about 1.5 times magnitude in longitudinal transport. Moreover, the oscillation of the spin density is slower in the transverse transport.

Usually, the charge-spin conversion efficiency is defined as $\alpha_{SH} = j_s/j_q$, where j_q and j_s are the charge current and generated pure spin current, respectively. In the following, we try to estimate the value of α_{SH} from the dynamic process. In the longitudinal transport, the polaron mainly drifts along chain 3 under the field. Similar as the case in a single polymer chain the velocity of the polaron is time dependent. After a short period of acceleration, a relative stable velocity is achieved, although slight fluctuation of the velocity still exists caused by interchain charge transfer. So we use the average velocity in a period of 1000 fs, where the traveled distance of the polaron can be easily obtained from the polaron center evolution. The average velocity is about 2.56 Å/fs. Thus, one may define the charge current as $j_q = e\nu$ with ν the average velocity of the polaron. But for the transverse transport, the continuous hopping is blocked by the boundary and brings difficulty in determining the current. Here we estimate the polaron average velocity within the first 43 fs at which the polaron just arrives at the boundary and the bounce has not happened yet. The transverse velocity can be calculated from the hopping distance of $4b$, which is about 0.39 Å/fs. Similar treatment has been also observed in another previous study to calculate

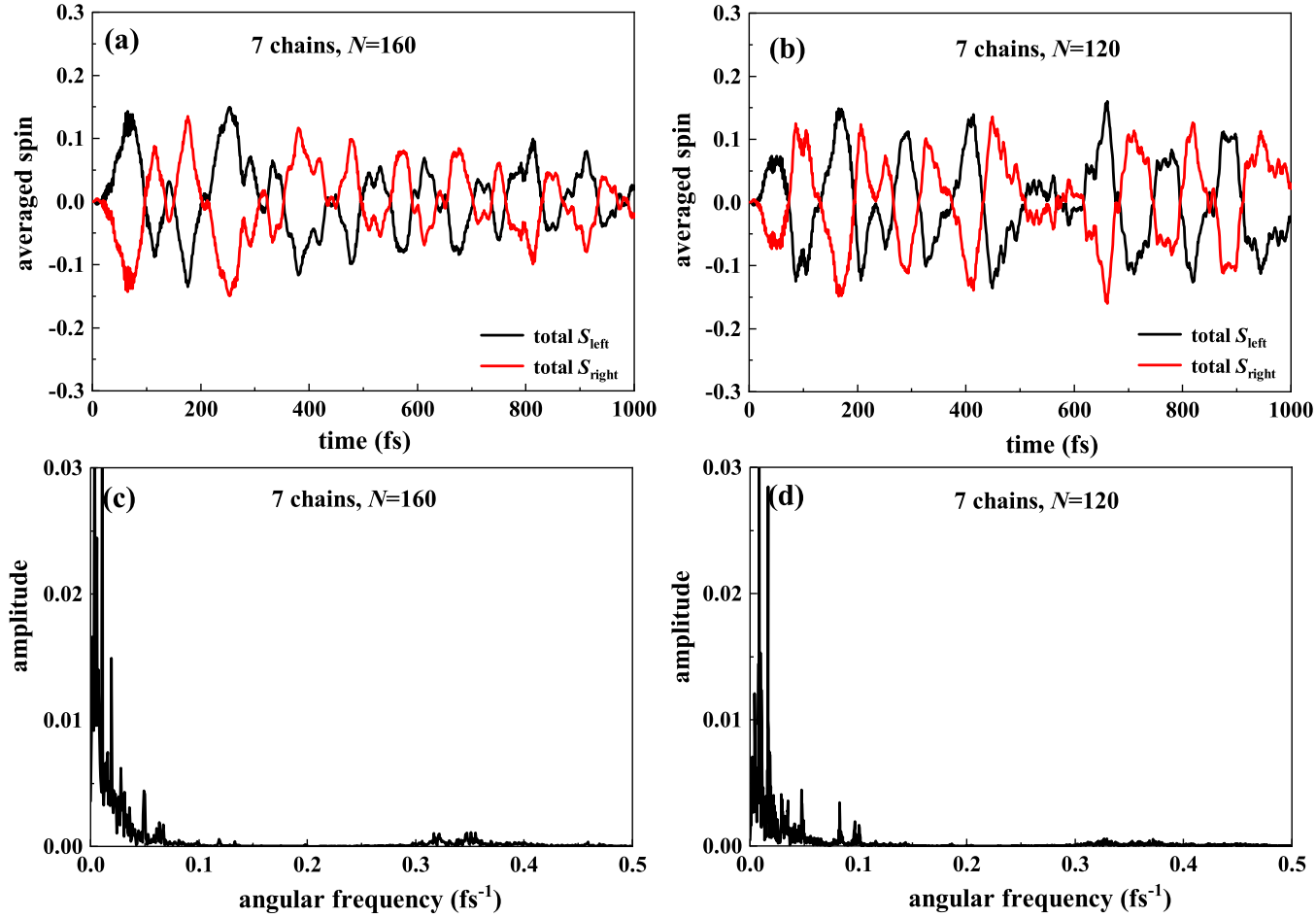

FIG. 9. Time-dependent evolution of the averaged spin and its FFT in seven chains. $N = 160$ for each chain in (a) and (c), and $N = 120$ for (b) and (d).

the velocity of interchain polaron transport [54]. The spin current is estimated as below. For the longitudinal transport, the spin current is defined as $j_s = (\frac{ds_1}{dt} + \frac{ds_2}{dt}) - (\frac{ds_4}{dt} + \frac{ds_5}{dt})$. Here

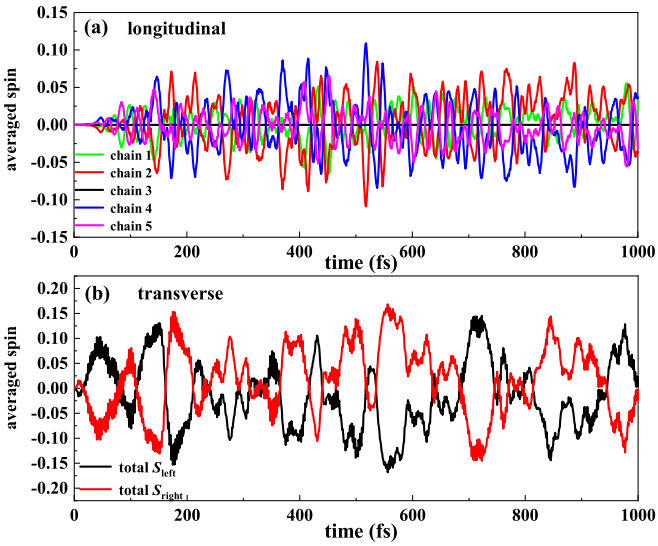

FIG. 10. Time-dependent evolution of the averaged spin for (a) longitudinal and (b) transverse polaron transport.

$s_{1(2,4,5)}$ is the averaged spins in chain 1(2,4,5) as shown in Fig. 10(a). For the transverse transport of the polaron, the spin current is $j_s = \frac{ds_L}{dt} - \frac{ds_R}{dt}$ with $s_{L(R)}$ the averaged total spin in the left and right moieties of the system shown in Fig. 10(b). For the oscillating SHE, we take the average of the absolute value of the spin current in 2000 fs to calculate the conversion efficiency. Eventually, the charge-spin conversion efficiency is gained as $\alpha_{SH}^{\parallel} = 0.005$ for the longitudinal transport and $\alpha_{SH}^{\perp} = 0.038$ for the transverse transport, respectively. The order of magnitude is comparable to that reported in organic ISHE measurement [34]. The result indicates that under the same electric field, the conversion efficiency for the transverse transport of polaron is much larger than that for the longitudinal transport.

To further investigate the relation between the charge-spin conversion efficiency and organic anisotropy, we calculate the ratio of charge-spin conversion efficiency for transverse and longitudinal polaron transport with different interchain coupling strengths. Here the strength of interchain SOC is also assumed to follow the change of the interchain coupling with $t^{\perp} = 4t_{so}^{\perp}$ and other parameters remain unchanged. The result is shown in Fig. 11. It is found that when $t^{\perp} = t_0$ is 0.04 ($t^{\perp} \sim 0.1$ eV), the conversion efficiency of the transverse transport is 5.6 times that of the longitudinal transport. The

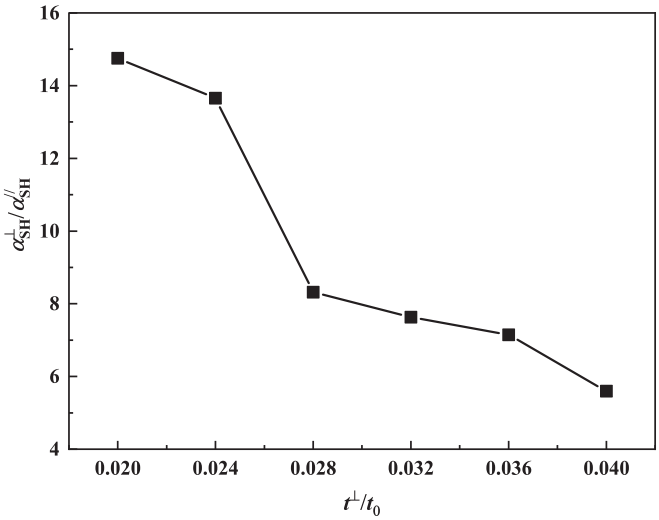

FIG. 11. Ratio of conversion efficiency for transverse ($\alpha_{SH}^{\perp}$) and longitudinal ($\alpha_{SH}^{\parallel}$) polaron transport with different interchain hopping integrals. Here t_0 is fixed as 2.5 eV.

ratio of conversion efficiency for the two transport directions increases quickly as the decrease of interchain coupling. As it decreases to 0.02 ($t^{\perp} \sim 0.05$ eV), that is, the anisotropy factor is increased by two times, the ratio of conversion efficiency changes to 14.8, where the merit of the transverse transport turns unusual. Note that the range of anisotropy investigated here is not large, since the present electric field cannot drive the polaron hopping between chains at an extremely weak interchain coupling. The situation of strong fields is not further expanded again.

Lastly, we would like to mention that the parameters used here are adopted from *trans*-polyacetylene as a typical polymer, and the polaron dynamics is investigated as the most interesting carrier in organic ISHE experiments. It is known that solitons are also possible excitations in *trans*-polyacetylene under doping, and even bipolaons exist in other nondegenerate polymers, depending on the species of polymers and the concentration of the dopant. Our previous work [43] has demonstrated that bipolarons may also cause the SHE in the case of intrachain transport. Considering the different charge and spin properties of each excitation [51], exploration of the interchain hopping process for other excitations under the SOC is also meaningful and needs to be expanded in the future. Furthermore, to achieve a longer hopping distance in a finite system, a polaron initially located in chain 1 is set. This is reasonable in the case of weak interchain coupling. An initial delocalized interchain polaron will arise if the interchain coupling strength turns larger [55]. Even in that case, the obtained picture is expected to still be valid since an interchain form of the polaron has emerged in present dynamic simulations.

IV. SUMMARY

The dynamic picture of the SHE in organic polymer ladders from interchain polarons hopping is revealed with a nonadiabatic dynamics method. The time evolution of charge and spin densities of polarons under a transverse electric field is traced in both transverse and longitudinal directions. The results show that in the finite system of five organic chains, polarons can jump from the first chain to the last chain in a very short time, and then oscillate around the edge in the form of an interchain polaron. During the interchain hopping of polarons, a directional longitudinal motion occurs for the polarons, which is always opposite for the spin-up and spin-down ones. Thus, a pure spin current along the longitudinal direction is obtained carried by polarons. By means of the statistical average over polarons with opposite initial spins, the time-dependent charges and spins in both the left and the right moieties of the system are calculated, where the criteria of SHE is confirmed and an obvious oscillating SHE is demonstrated. The oscillation of the SHE is analyzed from the FFT spectrum, which shows both a low-frequency part and a high-frequency part in the spectrum. The low-frequency part is attributed to the intrinsic electron dynamic oscillation in the finite-size system in the presence of polaron and the defined periodic boundary, while the high-frequency part is due to the spin-flip spin dynamics. In addition, we estimated the charge-spin conversion efficiency and compared it with that in the case of intrachain polaron transport. It is found that the conversion efficiency from the interchain transport may be larger than that from the intrachain transport by one order, which depends on the anisotropy factor of charge transport in various organics. This work reveals the microscopic picture of the SHE generated by interchain polaron hopping, and provides theoretical support to the enhancement of spin-charge conversion efficiency by organic anisotropy.

ACKNOWLEDGMENT

Support from the National Natural Science Foundation of China under Grants No. 11974215 and No. 12274264 is gratefully acknowledged.

[1] M. I. Dyakonov and V. I. Perel, JETP Lett. **13**, 467 (1971).
[2] M. I. Dyakonov and V. I. Perel, Phys. Lett. A **35**, 459 (1971).
[3] J. E. Hirsch, Phys. Rev. Lett. **83**, 1834 (1999).
[4] J. Sinova, D. Culcer, Q. Niu, N. A. Sinitsyn, T. Jungwirth, and A. H. MacDonald, Phys. Rev. Lett. **92**, 126603 (2004).
[5] J. Sinova, S. O. Valenzuela, J. Wunderlich, C. H. Back, and T. Jungwirth, Rev. Mod. Phys. **87**, 1213 (2015).
[6] T. Kimura, Y. Otani, T. Sato, S. Takahashi, and S. Maekawa, Phys. Rev. Lett. **98**, 156601 (2007).
[7] E. Saitoh, M. Ueda, H. Miyajima, and G. Tatara, Appl. Phys. Lett. **88**, 182509 (2006).
[8] K. Ando and E. Saitoh, Nat. Commun. **3**, 629 (2012).
[9] D. Wei, M. Obstbaum, M. Ribow, C. H. Back, and G. Woltersdorf, Nat. Commun. **5**, 3768 (2014).

[10] S. Murakami, N. Nagaosa, and S. C. Zhang, Science **301**, 1348 (2003).

[11] H.-A. Engel, B. I. Halperin, and E. I. Rashba, Phys. Rev. Lett. **95**, 166605 (2005).

[12] E. M. Hankiewicz and G. Vignale, Phys. Rev. B **73**, 115339 (2006).

[13] E. M. Hankiewicz, G. Vignale, and M. E. Flatté, Phys. Rev. Lett. **97**, 266601 (2006).

[14] W.-K. Tse and S. Das Sarma, Phys. Rev. B **75**, 045333 (2007).

[15] E. M. Hankiewicz and G. Vignale, Phys. Rev. Lett. **100**, 026602 (2008).

[16] Y. K. Kato, R. C. Myers, A. C. Gossard, and D. D. Awschalom, Science **306**, 1910 (2004).

[17] V. Sih, R. C. Myers, Y. K. Kato, W. H. Lau, A. C. Gossard, and D. D. Awschalom, Nat. Phys. **1**, 31 (2005).

[18] J. Wunderlich, B. Kaestner, J. Sinova, and T. Jungwirth, Phys. Rev. Lett. **94**, 047204 (2005).

[19] N. P. Stern, S. Ghosh, G. Xiang, M. Zhu, N. Samarth, and D. D. Awschalom, Phys. Rev. Lett. **97**, 126603 (2006).

[20] S. O. Valenzuela and M. Tinkham, Nature (London) **442**, 176 (2006).

[21] T. Tanaka, H. Kontani, M. Naito, T. Naito, D. S. Hirashima, K. Yamada, and J. Inoue, Phys. Rev. B **77**, 165117 (2008).

[22] L. Nuccio, M. Willis, L. Schulz, S. Fratini, F. Messina, M. D'Amico, F. L. Pratt, J. S. Lord, I. McKenzie, M. Loth, B. Purushothaman, J. Anthony, M. Heeney, R. M. Wilson, I. Hernández, M. Cannas, K. Sedlak, T. Kreouzis, W. P. Gillin, C. Bernhard, and A. J. Drew, Phys. Rev. Lett. **110**, 216602 (2013).

[23] S. Bandyopadhyay, Phys. Rev. B **81**, 153202 (2010).

[24] A. H. Castro Neto and F. Guinea, Phys. Rev. Lett. **103**, 026804 (2009).

[25] S. Schott, E. R. McNellis, C. B. Nielsen, H. Y. Chen, S. Watanabe, H. Tanaka, I. McCulloch, K. Takimiya, J. Sinova, and H. Sirringhaus, Nat. Commun. **8**, 15200 (2017).

[26] E. R. McNellis, S. Schott, H. Sirringhaus, and J. Sinova, Phys. Rev. Mater. **2**, 074405 (2018).

[27] T. Wakamura, F. Reale, P. Palczynski, S. Guéron, C. Mattevi, and H. Bouchiat, Phys. Rev. Lett. **120**, 106802 (2018).

[28] E. Vetter, I. VonWald, S. J. Yang, L. Yan, S. Koohfar, D. Kumah, Z. G. Yu, W. You, and D. L. Sun, Phys. Rev. Mater. **4**, 085603 (2020).

[29] Z. G. Yu, Phys. Rev. Lett. **106**, 106602 (2011).

[30] Z. G. Yu, Phys. Rev. B **85**, 115201 (2012).

[31] S. A. Wolf, D. D. Awschalom, R. A. Buhrman, J. M. Daughton, S. von Molnar, M. L. Roukes, A. Y. Chtchelkanova, and D. M. Treger, Science **294**, 1488 (2001).

[32] T. Dietl, H. Ohno, F. Matsukura, J. Cibert, and D. Ferrand, Science **287**, 1019 (2000).

[33] S. Watanabe, K. Ando, K. Kang, S. Mooser, Y. Vaynzof, H. Kurebayashi, E. Saitoh, and H. Sirringhaus, Nat. Phys. **10**, 308 (2014).

[34] K. Ando, S. Watanabe, S. Mooser, E. Saitoh, and H. Sirringhaus, Nat. Mater. **12**, 622 (2013).

[35] D. Sun, K. J. van Schooten, M. Kavand, H. Malissa, C. Zhang, M. Groesbeck, C. Boehme, and Z. Valy Vardeny, Nat. Mater. **15**, 863 (2016).

[36] M. M. Qaid, M. R. Mahani, J. Sinova, and G. Schmidt, Phys. Rev. Res. **2**, 013207 (2020).

[37] D. Sun, Y. Zhai, K. J. van Schooten, C. Zhang, M. Kavand, H. Malissa, M. Groesbeck, R. Menon, C. Boehme, and Z. V. Vardeny, J. Phys.: Condens. Matter **30**, 484003 (2018).

[38] Z. G. Yu, Phys. Rev. Lett. **115**, 026601 (2015).

[39] Q. X. Lu, S. Yin, T. Gao, W. Qin, S. J. Xie, F. Y. Qu, and A. Saxena, J. Phys. Chem. Lett. **11**, 1087 (2020).

[40] Q. X. Lu, S. J. Xie, and F. Y. Qu, J. Phys. Chem. Lett. **12**, 3540 (2021).

[41] W. P. Su, J. R. Schrieffer, and A. J. Heeger, Phys. Rev. Lett. **42**, 1698 (1979).

[42] G. C. Hu, Y. Y. Miao, and C. Timm, Phys. Rev. B **106**, 144309 (2022).

[43] Y. Y. Miao, D. Li, H. Q. Zhang, J. F. Ren, and G. C. Hu, Phys. Chem. Chem. Phys. **25**, 7763 (2023).

[44] Å. Johansson and S. Stafström, Phys. Rev. Lett. **86**, 3602 (2001).

[45] Å. Johansson and S. Stafström, Phys. Rev. B **66**, 085208 (2002).

[46] D. Obana, F. Liu, and K. Wakabayashi, Phys. Rev. B **100**, 075437 (2019).

[47] A. Mukherjee, A. Nandy, S. Sil, and A. Chakrabarti, Phys. Rev. B **105**, 035428 (2022).

[48] R. W. Brankin, I. Gladwell, and L. F. Shampine, RKSUITE: Software for ODE IVPS, http://www.netlib.org.

[49] A. A. Johansson and S. Stafström, Phys. Rev. B **69**, 235205 (2004).

[50] X. J. Liu, K. Gao, J. Y. Fu, Y. Li, J. H. Wei, and S. J. Xie, Phys. Rev. B **74**, 172301 (2006).

[51] A. J. Heeger, S. Kivelson, J. R. Schrieffer, and W.-P. Su, Rev. Mod. Phys. **60**, 781 (1998).

[52] J. Lei, H. Li, S. Yin, and S. J. Xie, J. Phys.: Condens. Matter **20**, 095201 (2008).

[53] Y. Y. Miao, H. J. Kan, D. Li, C. K. Wang, J. F. Ren, and G. C. Hu, Phys. Lett. A **433**, 128024 (2022).

[54] W. Liu, D. S. Liu, and H. H. Li, Acta Phys. Sin. **59**, 6405 (2010).

[55] H. A. Mizes and E. M. Conwell, Phys. Rev. Lett. **70**, 1505 (1993).